Research Square

Preprints are preliminary reports that have not undergone peer review.
They should not be considered conclusive, used to inform clinical practice,
or referenced by the media as validated information.

An Adaptive Method Based on the Atangana-Baleanu in the Sense of Caputo Fractional Operator for Improving Edge Detection Accuracy in SEM Images

Sergio Rengifo-Lozano

P880301324@unitru.edu.pe

National University of Trujillo

José Rodriguez-Melquiades

National University of Trujillo

Research Article

Keywords: Edge detection, Atangana–Baleanu fractional operator, adaptive fractional masks, scanning electron microscopy images, image processing

Posted Date: June 17th, 2026

DOI: https://doi.org/10.21203/rs.3.rs-9847540/v1

License: This work is licensed under a Creative Commons Attribution 4.0 International License.
Read Full License

Additional Declarations: No competing interests reported.

An Adaptive Method Based on the Atangana-Baleanu in the Sense of Caputo Fractional Operator for Improving Edge Detection Accuracy in SEM Images

Sergio Rengifo-Lozano[1*†] and José Rodriguez-Melquiades[1†]

[1*]Physics and Mathematics Science Faculty, National University of Trujillo, Av. Juan Pablo II s/n, Trujillo, La Libertad, 13011, Peru.

*Corresponding author(s). E-mail(s): P880301324@unitru.edu.pe;
Contributing authors: jrodriguez@unitru.edu.pe;
†These authors contributed equally to this work.

Abstract

Edge detection is a fundamental task in low-level image processing. Classical approaches such as the Roberts, Sobel, and Canny operators often perform poorly in the presence of noise and contrast variations, conditions that are common in scanning electron microscopy (SEM) images. To address these limitations, we propose ABC-AED, an adaptive edge detection method based on the Caputo-sense Atangana–Baleanu fractional operator. The associated Mittag–Leffler kernel introduces natural smoothing, non-local memory effects, and enhanced robustness to noise. The discrete fractional mask is constructed using finite-difference approximation combined with series expansion, allowing the fractional order to vary spatially. A bilateral filter preserves edge information while generating a local variance map that guides optimal block-wise assignment of fractional orders. ABC-AED is assessed against the Canny detector and a previously proposed fractional method using synthetic noisy images and real SEM data. Evaluations show that ABC-AED yields sharper and more continuous edges, maintains stability under noise, and ensures consistent detection across SEM images with varying contrast. Overall, ABC-AED outperforms competing methods, which exhibit edge distortion, fragmentation, or excessive blurring, although slight contour smoothing remains.

Keywords: Edge detection, Atangana–Baleanu fractional operator, adaptive fractional masks, scanning electron microscopy images, image processing

1 Introduction

Image processing has traditionally relied on edge detection operators, which are based on identifying abrupt variations in the intensity of the pixels within an image [1]. Classical edge detection techniques, such as the Roberts, Sobel, and Canny operators, employ first- and second-order derivatives to extract contour information. Although these methods have demonstrated satisfactory performance in many applications, they exhibit notable limitations when applied to images with complex characteristics, including strong contrast variations and significant noise levels [2]. Such limitations are commonly reflected in reduced robustness to noise and difficulties in preserving fine structural details, ultimately compromising edge detection accuracy.

In order to overcome these drawbacks, the use of fractional calculus in the design of edge detection operators has gained increasing attention. In particular, [3] investigated the construction of edge detection masks based on fractional-order operators, showing that fractional approaches can substantially enhance edge detection performance under noisy conditions and varying contrast levels.

A critical aspect of fractional-order edge detection lies in the selection of the fractional order itself. This choice plays a decisive role in balancing edge enhancement and noise suppression, as it directly influences the sharpness of detected edges and the robustness of the operator against noise. An inappropriate selection of the fractional order may result in blurred or poorly defined edges, or may amplify noise, thereby reducing the overall effectiveness of the detection process.

Recent studies [4][5] have demonstrated that the optimal fractional order is not spatially uniform across an image, but rather depends on the local characteristics of different regions. Consequently, distinct areas within the same image may require different fractional orders to achieve optimal edge detection. This observation highlights the intrinsic complexity of the problem and underscores the need for adaptive strategies capable of adjusting the fractional order in response to local image variations.

Within this framework, [6] proposed an adaptive edge detection method based on the analysis of local pixel intensity variance. Although this approach constitutes a significant advancement, [7] identified several limitations associated with relying exclusively on local variance for image segmentation, including:

- **Noise sensitivity:** Local information, including local variance, is highly susceptible to noise, especially in images with high noise density, which can lead to faulty segmentation.
- **Sub-segmentation:** In the presence of intense noise, the exclusive use of local information can lead to under-segmentation, as noisy pixels may be misinterpreted as relevant information and retained during the clustering process
- **Loss of detail and blurred edges:** Excessive smoothing combined with noise can cause the loss of fine details and the diffusion of edges, making it difficult to accurately identify boundaries.
- **Difficulty in managing homogeneity:** When pixels within a local window are homogeneous or located at the boundaries of different objects, algorithms may fail to correctly classify those pixels, affecting the quality of segmentation.

These limitations become more relevant in contexts where image quality is compromised from the acquisition process onward. Such is the case with images obtained using scanning electron microscopy (SEM), which are generated by scanning a beam of electrons point by point over the sample. Although detailed, this procedure introduces various unwanted artifacts and noise that hinder accurate edge segmentation [8].

According to [9], these noises can be classified into different types, including:

- **Detector noise:** Caused by limitations in the signal detection and digitization system; it consists of a combination of electronic and Gaussian noise.
- **Distortions caused by scanning:** They include effects such as displacement or deformation caused by the return of the probe and the scanning speed.
- **Acquisition noise:** Such as blurring due to rapid scanning, line errors, beam instability (jitter), and the appearance of random black or white pixels.
- **Saturation and quantization noise:** Generated when pixel values exceed the sensor's capacity or due to errors in analog-to-digital conversion.

In this context, we develop an edge detection method based on the Atangana–Baleanu fractional operator in the Caputo sense (ABC) to improve edge detection accuracy in scanning electron microscopy (SEM) images. First, the ABC fractional operator is introduced and discussed from a qualitative perspective, highlighting its suitability for analyzing noisy images. Based on this operator, we construct an adaptive edge detection mask and, for comparison, an additional adaptive mask derived from the framework proposed in [6].

Both masks are applied to natural images from the Berkeley Segmentation Dataset [10] as well as to SEM images reported in [11]. The performance of the proposed method is quantitatively evaluated using standard metrics, including the Jaccard index, F1-score, precision, and recall. Finally, the obtained results are analyzed and compared, allowing us to discuss the main advantages and limitations of the proposed adaptive fractional edge detection approach.

The article is organized as follows: Section 2 presents the proposed ABC-AED method. We first analyze the Atangana–Baleanu fractional operator in the Caputo sense (ABC) and develop a fractional edge detection mask that exploits its smoothing properties and memory effects. An adaptive algorithm is then introduced to compute the optimal fractional order for edge detection. Section 3 describes the application of the fractional masks on three types of images: natural images, natural images with synthetic mixed noise, and SEM images. This section also presents a comparative evaluation of ABC-AED against the fractional approach proposed by [6] and the classical Canny method, highlighting both qualitative and quantitative differences. Section 4 discusses the observed differences and their practical implications. Finally, Section 5 concludes the work and summarizes the main findings.

2 Methods

2.1 Atanga-Baleanu Fractional Operator in the Caputo Sense

The fractional derivative can be interpreted as a convolution between the derivative of a function in Sobolev space and a kernel constructed from exponential functions,

such as the Mittag-Leffler function [12]. In particular, [13] present this formulation through the ABC operator.

Given $f \in H^1(0,1)$ and $0 < \alpha < 1$, the fractional derivative of Atangana-Baleanu in the Caputo sense is defined as:

$$
\begin{aligned}
{}_0^{ABC}D_t^{\alpha} f(t) = \\
\frac{B(\alpha)}{1-\alpha} \int_0^t \frac{d}{d\tau}\{f(\tau)\} E_{\alpha}\left[-\frac{\alpha}{1-\alpha}(t-\tau)^{\alpha}\right] d\tau
\end{aligned}
\tag{1}
$$

where $B(\alpha) > 0$ is a normalization function denoted by:

$$
B(\alpha) = 1 - \alpha + \frac{\alpha}{\Gamma(\alpha)} \tag{2}
$$

and $E_{\alpha}(\cdot)$ is the Mittag-Leffler function of one variable, given by:

$$
E_{\alpha}(t) = \sum_{k=0}^{\infty} \frac{t^k}{\Gamma(\alpha k + 1)}, \quad \alpha > 0 \tag{3}
$$

The fractional integral is defined by:

$$
\begin{aligned}
{}_0^{ABC}I_t^{\alpha} f(t) = & \frac{1-\alpha}{B(\alpha)} f(t) \\
& + \frac{\alpha}{B(\alpha)\Gamma(\alpha)} \int_0^t f(\tau)(t-\tau)^{\alpha-1}\, d\tau
\end{aligned}
\tag{4}
$$

The fact that f is defined in Sobolev space implies that both the function and its derivatives, in the weak sense, are integrable functions. This can be interpreted as robustness against singularities, insofar as these are integrable in the Lebesgue sense. As a consequence of this property, we have that $H^1(0,1) \subset L^2(0,1)$ [14].

On the other hand, according to [15], the Mittag-Leffler function $E_{\alpha}(-x)$, with $x > 0$ and $0 < \alpha < 1$, has the property of being completely monotonic. This characteristic is present in the definition of the ABC fractional derivative, and it is precisely what gives the operator its memory and nonlocal attenuation properties [12].

Additionally, taking advantage of the inclusion $H^1(0,1) \subset L^2(0,1)$ and the definition of the ABC fractional derivative, it is possible to rewrite this derivative in terms of a convolution, expressed by the following equation:

$$
{}_0^{ABC}D_t^{\alpha} f(t) = \frac{B(\alpha)}{1-\alpha} \cdot \left[\frac{df(t)}{dt} * E_{\alpha}\left(-\frac{\alpha}{1-\alpha} t^{\alpha}\right)\right] \tag{5}
$$

The Mittag–Leffler kernel determines how the weight of the rate of change is distributed over time. Its decay, slower than that of an exponential but faster than that of a power law, generates an intermediate memory effect. Thus, past values of the original function maintain a significant influence on the convolution at later times, reflecting the system's ability to retain information from previous states.

2.2 Qualitative Properties for Noisy Signal Analysis

As mentioned earlier, SEM images are characterized by the presence of significant noise components. To illustrate the effectiveness of the ABC fractional operator in the presence of noise, we consider a one-dimensional noisy signal defined as follows:

$$x(t) = \sum_k a_k \, \delta(t - t_k) \,, \tag{6}$$

where t_k denote the event times, a_k are random amplitudes, and δ denotes the Dirac delta distribution.

Now, suppose that $x(t) \in (0, 1)$. The classical derivative of $x(t)$ is given by

$$\frac{dx(t)}{dt} = \frac{d}{dt} \sum_k a_k \, \delta(t - t_k) = \sum_k a_k \, \frac{d}{dt} \delta(t - t_k) \,. \tag{7}$$

Now, using the definition of the ABC fractional derivative, the fractional derivative of a noisy signal $x(t)$ can be expressed as

$$\begin{aligned} {}_0^{ABC}D_t^{\alpha} x(t) = \frac{B(\alpha)}{1-\alpha} \int_0^t \left(\sum_k a_k \frac{d}{d\tau} \delta(\tau - \tau_k) \right) \\ E_\alpha \left[-\frac{\alpha}{1-\alpha} (t-\tau)^\alpha \right] d\tau, \end{aligned} \tag{8}$$

where $\alpha \in (0, 1)$ and $B(\alpha)$ is the normalization function associated with the ABC operator and $E_\alpha(\cdot)$ denotes the Mittag-Leffler function.

For convenience, we define $g_k(t, \tau) = a_k E_\alpha \left[-\frac{\alpha}{1-\alpha} (t-\tau)^\alpha \right]$ and use the property $h(\tau) \, \delta'(\tau - \tau_k) = h(\tau_k) \, \delta'(\tau - \tau_k) - h'(\tau_k) \, \delta(\tau - \tau_k)$. The fractional derivative in (14) can be rewritten as

$${}_0^{ABC}D_t^{\alpha} x(t) = \frac{B(\alpha)}{1-\alpha} \int_0^t \left(\sum_k g_k(t, \tau) \, \delta'(\tau - \tau_k) \right) d\tau. \tag{9}$$

Expanding the previous equation, we obtain

$$\begin{aligned} {}_0^{ABC}D_t^{\alpha} x(t) = & \frac{B(\alpha)}{1-\alpha} \Bigg\{ \int_0^t \left(\sum_k g_k(t, \tau_k) \, \delta'(\tau - \tau_k) \right) d\tau \\ & - \sum_k \partial_\tau g_k(t, \tau_k) \, \mathbb{1}_{(0,t)}(\tau_k) \Bigg\}, \end{aligned} \tag{10}$$

where $\mathbb{1}_{(0,t)}(\cdot)$ denotes the indicator function over the interval $(0, t)$.

Since $g_k(t, \tau_k)$ is constant with respect to τ, and considering distributions over $(0, t)$ with test functions vanishing at the boundaries, the first integral term in (10)

vanishes, i.e.,

$$\int_0^t \left(\sum_k g_k(t, \tau_k)\, \delta'(\tau - \tau_k) \right) d\tau = 0. \tag{11}$$

Therefore, the ABC fractional derivative of a noisy signal reduces to

$$\begin{aligned} {}_0^{ABC}D_t^{\alpha} x(t) = -\frac{B(\alpha)}{1-\alpha} \\ \sum_{\substack{k \\ 0<\tau_k<t}} a_k \, \frac{\partial}{\partial \tau} E_\alpha \left[-\frac{\alpha}{1-\alpha}(t-\tau)^\alpha \right] \Big|_{\tau=\tau_k}. \end{aligned} \tag{12}$$

Finally, differentiating the Mittag-Leffler function with respect to τ, we obtain

$$\begin{aligned} &\frac{\partial}{\partial \tau} E_\alpha \left[-\frac{\alpha}{1-\alpha}(t-\tau)^\alpha \right] \\ &\quad = \sum_{n=1}^{\infty} \frac{-\alpha n}{\Gamma(\alpha n + 1)} \left(-\frac{\alpha}{1-\alpha} \right)^n (t-\tau)^{\alpha n - 1}. \end{aligned} \tag{13}$$

The corresponding expression for the ABC fractional derivative of $x(t)$ is given by

$$\begin{aligned} {}_0^{ABC}D_t^{\alpha} x(t) = -\frac{B(\alpha)}{1-\alpha} \sum_{\substack{k \\ 0<\tau_k<t}} \sum_{n=1}^{\infty} \\ \left[-\frac{a_k\, \alpha n}{\Gamma(\alpha n + 1)} \left(-\frac{\alpha}{1-\alpha} \right)^n (t-\tau_k)^{\alpha n - 1} \right], \end{aligned} \tag{14}$$

where $\alpha \in (0, 1)$

By comparing the classical and fractional derivatives of the noisy signal, it can be observed that the classical approach introduces singularities through the term $\frac{d}{dt}\delta(t - t_k)$. This term is not integrable in a neighborhood of t_k and lacks memory, since the derivative at time t depends solely on the instantaneous value of the signal.

In contrast, the fractional approach exhibits a smoothing behavior: the corresponding derivative is continuous and differentiable, and it inherently incorporates a memory effect. Specifically, the value of the fractional derivative at time t accounts for the contribution of all past events satisfying $t_k < t$, modulated by the smooth kernel $(t - \tau_k)^{\alpha n - 1}$.

2.3 Construction of Fractional Edge Detection Mask

Using the expression in (5) and applying the theorem of integral additivity, the expression can be rewritten as follows:

$$
{}_0^{ABC}D_t^{\alpha} f(t) = \frac{B(\alpha)}{1-\alpha}\left\{ \sum_{k=0}^{L-1} \int_{\frac{kt}{L}}^{\frac{kt+t}{L}} \frac{d}{d\tau}\{f(t-\tau) \right.
$$
$$
\left. E_{\alpha}\left(-\frac{\alpha}{1-\alpha}\,\tau^{\alpha}\right)\, d\tau \right\}. \tag{15}
$$

Using the backward finite difference approximation for the derivative, together with several properties of the Gamma and Mittag–Leffler functions, the expression of the ABC fractional operator can be written as follows.

$$
\begin{aligned}
&{}_0^{ABC}D_t^{\alpha} f(t) = \\
&\quad \frac{B(\alpha)}{1-\alpha}\Bigg\{ f(t)\, E_{\alpha,2}(-\lambda h^{\alpha}) \\
&\qquad + \sum_{k=1}^{L-1} \Big[(k+1)E_{\alpha,2}(-\lambda(k+1)^{\alpha}h^{\alpha}) \\
&\qquad - 2kE_{\alpha,2}(-\lambda(kh)^{\alpha}) \\
&\qquad + (k-1)E_{\alpha,2}(-\lambda(k-1)^{\alpha}h^{\alpha}) \Big] f(t-kh) \\
&\qquad + \Big[(L-1)E_{\alpha,2}(-\lambda(L-1)^{\alpha}h^{\alpha}) \\
&\qquad - LE_{\alpha,2}(-\lambda(Lh)^{\alpha}) \Big] f(t-Lh) \Bigg\}.
\end{aligned} \tag{16}
$$

We can express (16) in a compact form as ${}_0^{ABC}D_t^{\alpha} f(t) = \frac{B(\alpha)}{1-\alpha} \sum_{k=0}^{L} \mathcal{A}(k)\, f(t-kh)$, where $\mathcal{A}(k)$ represents the summation coefficients that lead to the construction of the fractional mask, defined as follows:

$$
\mathcal{A}(k) = \begin{cases} E_{\alpha,2}\big(-\lambda \left(\frac{t}{2}\right)^{\alpha}\big), & k = 0, \\ 2E_{\alpha,2}\big(-\lambda 2^{\alpha} \left(\frac{t}{2}\right)^{\alpha}\big) - 2E_{\alpha,2}\big(-\lambda \left(\frac{t}{2}\right)^{\alpha}\big), & k = 1, \\ E_{\alpha,2}\big(-\lambda \left(\frac{t}{2}\right)^{\alpha}\big) - 2E_{\alpha,2}\big(-\lambda 2^{\alpha} \left(\frac{t}{2}\right)^{\alpha}\big), & k = 2. \end{cases} \tag{17}
$$

for $L = 2$.

By expanding the Mittag–Leffler function into the first three terms of its series representation, the resulting coefficients are given by:

$$
\begin{cases} p_0 = 1 - \dfrac{\lambda 2^{-\alpha}}{\Gamma(\alpha+2)} t^{\alpha} + \dfrac{\lambda^2 2^{-2\alpha}}{\Gamma(\alpha+2)} t^{2\alpha}, \\ p_1 = \dfrac{2\lambda(2^{-2\alpha}-1)}{\Gamma(\alpha+2)} t^{\alpha} + \dfrac{2\lambda^2(1-2^{-2\alpha})}{\Gamma(\alpha+2)} t^{2\alpha}, \\ p_2 = -1 + \dfrac{\lambda(2-2^{-\alpha})}{\Gamma(\alpha+2)} t^{\alpha} - \dfrac{\lambda^2(2^{-2\alpha}-2)}{\Gamma(\alpha+2)} t^{2\alpha}. \end{cases} \tag{18}
$$

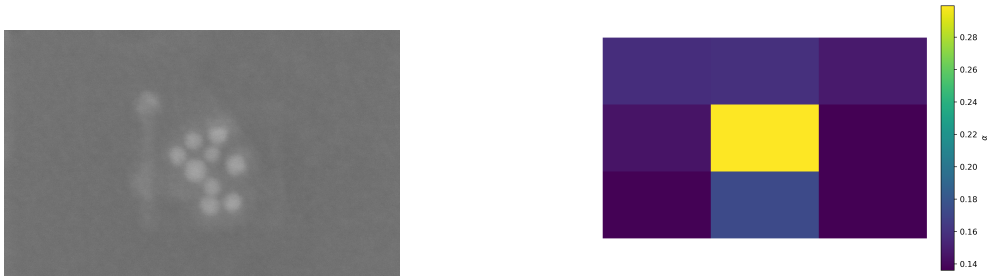
By interpreting the time step t as the discrete unit of spatial displacement in the digital image, corresponding to the step between pixels, the operator is evaluated at $t = 1$. Consequently, the coefficients are reduced to constant values, which define the discrete fractional mask used for the numerical implementation of the ABC operator.

Using the mask structure proposed in [16], which is based on the central derivative and the tensor product [17], and considering the Mittag–Leffler expansion together with the normalization included in the definition of the ABC fractional operator, the following fractional masks are obtained:

$$h_x = \begin{bmatrix} -\rho_0 & 0 & \rho_0 \\ -\rho_1 & 0 & \rho_1 \\ -\rho_2 & 0 & \rho_2 \end{bmatrix}, \quad h_y = \begin{bmatrix} \rho_0 & \rho_1 & \rho_2 \\ 0 & 0 & 0 \\ -\rho_0 & -\rho_1 & -\rho_2 \end{bmatrix},$$

where h_x and h_y represent the horizontal and vertical components, respectively, and the fractional coefficients ρ_0, ρ_1, and ρ_2 are obtained from the polynomials p_0, p_1, and p_2, respectively, according to:

$$\begin{bmatrix} \rho_0 \\ \rho_1 \\ \rho_2 \end{bmatrix} = \frac{B(\alpha)}{1-\alpha} \cdot \begin{bmatrix} p_0 \\ p_1 \\ p_2 \end{bmatrix}, \quad \lambda = \frac{\alpha}{1-\alpha}, \quad \alpha \in (0,1). \tag{19}$$



(a) SEM image (b) Spatial distribution of α

Fig. 1: Visualization of the spatial distribution of α in the SEM image.

2.4 Development of the Proposed Adaptive Property

Building upon the studies of [4] and [16], which demonstrate that the optimal fractional order is spatially variant and depends on local image characteristics, we propose an adaptive strategy to account for this variability.

Specifically, we introduce a methodology based on the construction of a normalized grid of fractional-order values. The procedure is described as follows:

1. Consider a normalized grayscale image

$$I \in [0,1]^{H \times W},$$

where H and W denote the height and width of the image in pixels, respectively.

2. Apply a bilateral filter to the image I, yielding

$$J \leftarrow \mathscr{B}(I).$$

3. Compute the map D as the absolute value of the pointwise product between I and J:

$$D(p) \leftarrow |I(p)\, J(p)|\,, \quad p \in \Omega.$$

4. Initialize the fractional-order map α as a zero matrix of size $H \times W$.
5. For each block $\Omega_{m,n}$ of size $h \times w$, determined from $\mathrm{mcd}(H, W)$ and traversed with step (h, w):

   - Compute the local average value:

$$\mu_{m,n} \leftarrow \frac{1}{|\Omega_{m,n}|} \sum_{p \in \Omega_{m,n}} D(p).$$

   - Determine the adaptive fractional order:

$$\alpha_{m,n} \leftarrow \alpha_{\min} + (\alpha_{\max} - \alpha_{\min}) \cdot \mu_{m,n}.$$

   - Assign the value $\alpha_{m,n}$ to all pixels within the block $\Omega_{m,n}$.

6. Return the resulting fractional-order map α.

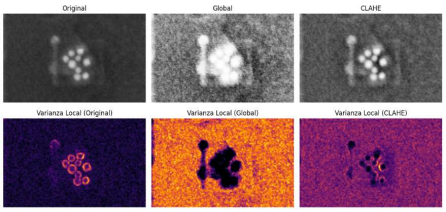
Fig 1 illustrates the application of the proposed algorithm, which yields the α-grid shown in Figure 1b. This grid represents the spatial distribution of the fractional-order parameter α across the image, as depicted in Figure 1a. Notably, the SEM image exhibits a higher concentration of nanoparticles in the central region, which is consistently reflected by larger fractional-order values compared to the background regions.

2.5 Algorithmic Formulation and Complexity Analysis

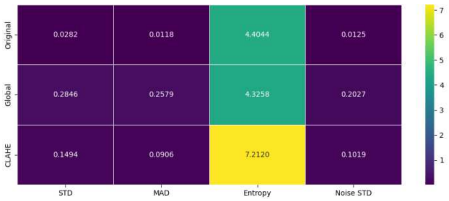
The proposed algorithm consists of four main stages. The first corresponds to image loading and preprocessing. Since the edge detectors are intended for application to SEM images, which exhibit structural noise [9], the equalization step has been deliberately omitted. This is because such techniques require images with a low noise level to be effective. Furthermore, according to [18], modern adaptive equalization methods, although superior to classical approaches, tend to thicken edges and amplify the noise present, as shown in Figure 2a.

Figure 2b shows that, although CLAHE can visually improve contrast while preserving the image structure, the increase in information, reflected in the entropy, is accompanied by a rise in noise, which constitutes a disadvantage for its mitigation.

Algorithm 1 describes the loading and preprocessing procedure, which includes grayscale conversion and normalization.



(a) Results of applying global equalization and adaptive equalization (CLAHE) to a SEM image with non-deterministic noise.



(b) Comparison of the effect of global and adaptive equalization (CLAHE) on a SEM image.

Fig. 2: Comparison of the effect of global and adaptive equalization (CLAHE) on a SEM image.

The second stage consists of computing a minimum area based on the greatest common divisor (GCD) criterion, in order to obtain a partition proportional to the overall size of the image. This procedure is formalized in Algorithm 2.

In the third stage, from the minimum area defined previously, fractional values are computed for each region of that size as a function of the local image content. This process exploits the properties of bilateral filtering, which preserves edges while attenuating noise. This procedure is outlined in Algorithm 3.

The final stage aims to generate the edge map of the image. In this stage, fractional masks are employed that incorporate the coefficients defined in (19), whose implementation is detailed in Algorithm 4.

2.5.1 Analysis of Algorithm Complexity

Let $W \times H$ be the size of the input image.

- **Loading and preprocessing:** Grayscale conversion, when required, and normalization correspond to point-wise operations that traverse the image exactly once. Therefore, this stage has complexity $\mathcal{O}(WH)$.
- **Minimum area computation:** The greatest common divisor $\gcd(h, w)$ is computed using the Euclidean algorithm with complexity $\mathcal{O}(\log \min(h, w))$. Since this operation is performed only once and does not depend on the number of pixels, its cost is considered constant, $\mathcal{O}(1)$.
- **Adaptive α grid computation:** First, bilateral filtering is applied with complexity $\mathcal{O}(WH \cdot k^2)$, where k is the window size. Assuming k is constant, this operation reduces to $\mathcal{O}(WH)$. Subsequently, the image is divided into blocks of size $h_t \times w_t$, generating approximately $\frac{WH}{h_t w_t}$ blocks. Computing the average within each block requires $\mathcal{O}(h_t w_t)$ operations, which leads to an overall linear complexity of $\mathcal{O}(WH)$.
- **Edge computation:** The gradients g_x and g_y are obtained via convolutions with 3×3 masks, which implies a constant number of operations per pixel and therefore complexity $\mathcal{O}(WH)$. The bilateral filtering applied afterwards maintains the same order of complexity under the constant-window assumption. Finally, the gradient magnitude is computed point-wise, preserving linear complexity.

Since all dominant stages scale linearly with the number of pixels, the total complexity of the proposed algorithm is $\mathcal{O}(WH)$.

3 Results

3.1 Application of Fractional Masks

The computational experiment is structured into three distinct stages. In Stage 1, the edge detection methods are applied to natural images from the dataset reported in [10], which provides ground truth annotations for quantitative accuracy evaluation. Stage 2 assesses the robustness of the methods by introducing different types of noise, including Gaussian, salt-and-pepper, speckle, and Poisson, into the images from Stage 1. Stage 3 involves the analysis of SEM images from the dataset presented in [11]. Since this dataset lacks ground truth annotations, these were manually generated to enable quantitative evaluation using objective metrics. Across all stages, the performance of three methods is systematically compared: Canny's edge detector, the method proposed in [6] (hereafter referred to as the Hacini method), and the ABC-AED method introduced in this work.

3.1.1 Stage 1

For this stage, the images *Hawk* and *House* from the dataset [19] were used, as shown in Fig. 3a and 3b, respectively.



(a) Hawk (b) House

Fig. 3: Study images of Stage 1

After applying the edge detection masks corresponding to Canny, the method proposed in [6], and the ABC-AED method, the results shown in Fig. 4 were obtained.

Visual inspection indicates that the ABC-AED method produces more defined and consistent edges, although some blurring is observed in certain regions. The Canny detector, by contrast, preserves a larger amount of fine detail. The method proposed in [6], however, demonstrates the most limited performance, failing to adequately detect edges in the analyzed images.



(a) Edge detection of *Hawk*

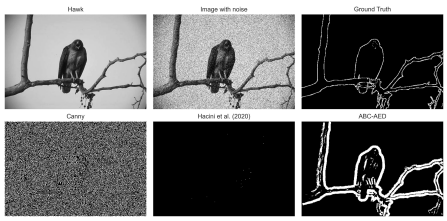


(b) Edge detection of *House*

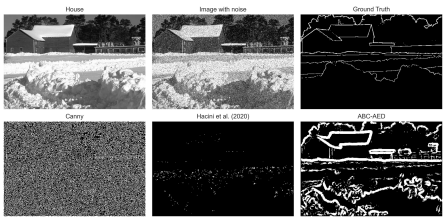
Fig. 4: Edge detection results for Stage 1 images. From left to right: the original grayscale image, the ground truth, the edge map obtained using the Hacini method, the ABC-AED edge map, and the Canny edge map.

3.1.2 Stage 2

For this stage, the same images used in Stage 1 were employed, with the addition of combined noise. Specifically, Gaussian, salt and pepper, speckle, and Poisson noise were introduced. The resulting edge detection outputs are presented in Figure 5.



(a) Edge detection of *Hawk* with noise



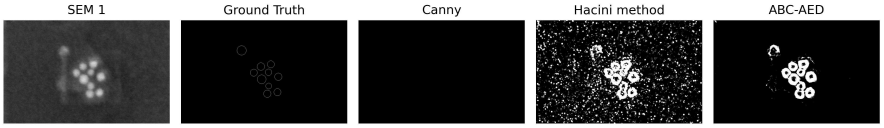
(b) Edge detection of *House* with noise

Fig. 5: Results of edge detection for the images corresponding to Stage 2. First row (from left to right): the original grayscale image, the image with combined noise, and the ground truth. Second row (from left to right): the Canny edge map, the edge map obtained using the Hacini method, and the ABC-AED edge map.

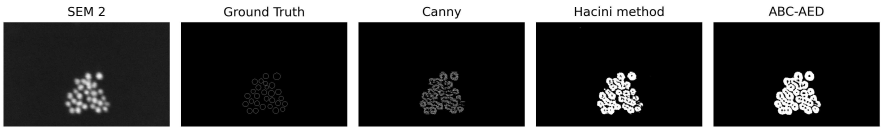
Canny's method is observed to be sensitive to noise. The method proposed in [6] exhibits limitations in edge detection. In contrast, the ABC-AED method demonstrates robustness to noise and successfully identifies edges, although some blurring is present.

3.1.3 Stage 3

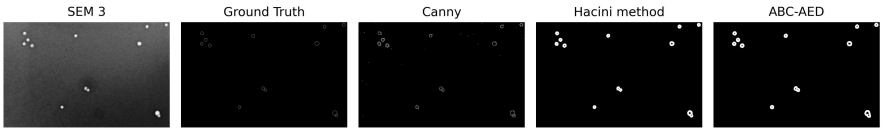
In this final stage, SEM images from the dataset reported in [11] were used. The edge detection results are presented in Figure 6.



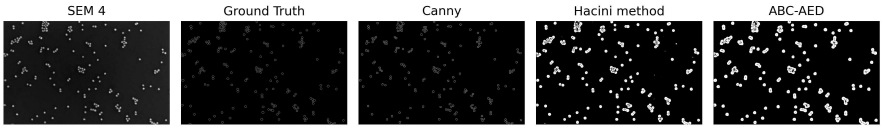
(a) Edge detection on *SEM 1*



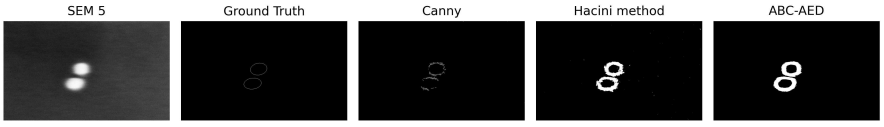
(b) Edge detection on *SEM 2*



(c) Edge detection on *SEM 3*



(d) Edge detection on *SEM 4*



(e) Edge detection on *SEM 5*

Fig. 6: Edge detection results for the Stage 3 images. From left to right: the original grayscale image, the ground truth, the Canny edge map, the edge map obtained by the Hacini method, and the ABC-AED edge map.

Visual inspection suggests that the Canny method does not adequately detect edges in SEM image 1, which exhibits low contrast and diffuse contours. The method proposed by [6] identifies the edges, although it also allows noise to pass through. The best performance corresponds to the ABC-AED method, as it captures a greater number of edges while effectively attenuating noise.

In SEM image 2, the Canny method detects edges in a fragmented and discontinuous manner, whereas the methods of [6] and ABC-AED yield similar and more consistent results.

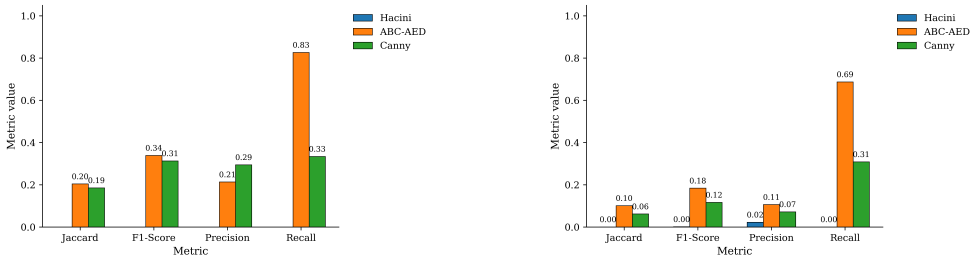
In SEM image 3, the Canny method identifies finer edges, although it fails to completely eliminate noise. In contrast, the methods of [6] and ABC-AED exhibit comparable performance to each other.

In SEM image 4, characterized by containing numerous objects of interest, Canny shows better overall performance, although some edge discontinuity remains. On the other hand, the methods of [6] and ABC-AED produce thicker edges, causing overlap between some elements.

Finally, in SEM image 5, Canny exhibits incomplete edges, while the method of [6] detects contours irregularly, partially distorting the object. In contrast, ABC-AED better preserves both the contour and the edge structure of the image.

3.2 Quantitative Results and Comparison

For quantitative evaluation, the edge maps obtained at each stage were compared against their respective ground truths using the Jaccard index, Precision-Recall (PR) metrics, and the F1-Score. The Jaccard index quantifies the overall similarity between the predicted map and the reference, while PR characterizes the trade-off between false positives and false negatives. The F1-Score combines precision and recall into a single metric, providing a compact measure of overall performance [20, 21].



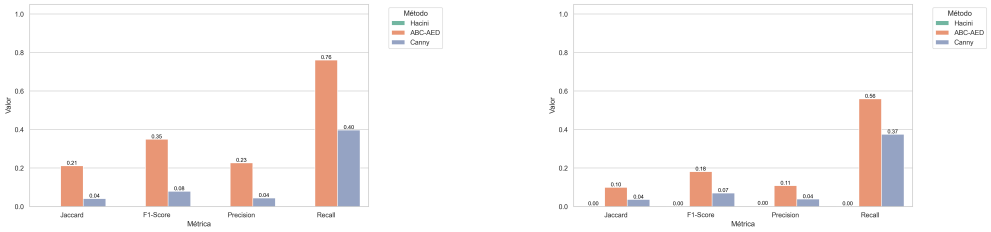
(a) Metrics for *Hawk* (b) Metrics for *House*

Fig. 7: Accuracy of the edge maps for the Stage 1 images.

In Stage 1, the obtained metrics are moderate but allow the relative performance of the evaluated methods to be clearly distinguished. The Hacini method fails to detect relevant edges in any of the images, which is reflected in values close to zero across all metrics. In contrast, the Canny method shows some level of detection, albeit with a marked imbalance towards low recall, indicating a significant loss of true edges. The proposed ABC-AED method achieves the highest values in both the Jaccard index and the F1-score, demonstrating a better balance between precision and recall. These results suggest that, despite the variability in contrast and texture characteristic of

natural images, ABC-AED maintains greater consistency in edge detection compared to the other approaches, as illustrated in Figures 7a and 7b.

In Stage 2, the results show consistent behavior across the compared approaches. The Hacini method maintains metrics close to zero for all noise types, confirming its lack of adaptability under noisy conditions. Canny presents a slight increase in recall, indicating a greater capacity to detect additional edges; however, its precision remains low, implying a high false positive rate and, consequently, reduced F1-score values. In contrast, the proposed ABC-AED method maintains the highest values in both the Jaccard index and the F1-score, reflecting greater stability against noise-induced perturbations. Although some blurring is observed in the detected edges, the balance achieved between precision and recall highlights the superiority of the proposed method in terms of robustness, as shown in Figures 8a and 8b.



(a) Metrics for *Hawk* with noise

(b) Metrics for *House* with noise

Fig. 8: Accuracy of the edge maps for the Stage 2 images.

In Stage 3, the results show that the performance of the methods strongly depends on the morphological characteristics and contrast present in each SEM image. In image 9a, the Canny operator failed to detect relevant edges, while the Hacini and ABC-AED methods achieved high recall values (0.94 and 0.93, respectively), indicating greater sensitivity in recovering diffuse contours. In 9b, all three methods showed comparable performance, with a slight advantage for Hacini and Canny in terms of Jaccard and F1-score. For images 9c, 9d, and 9e, corresponding to structures with better-defined contours, the Canny method achieved the best overall results, particularly in SEM 4, where it obtained the maximum values of Jaccard (0.25), F1-score (0.40), and precision (0.37). On the other hand, Hacini consistently maintained high recall values across all images, albeit accompanied by low precision, suggesting a tendency towards edge over-detection. Taken together, these results indicate that ABC-AED and Hacini exhibit greater sensitivity in images with faint edges, while Canny offers a better balance between precision and recall when contours are better defined. All quantitative results are summarized in Table 1.

Stage	Image	Method	Metrics			
			Jaccard	F1	Prec.	Rec.
1	Hawk	Hacini	0.00	0.00	0.00	0.00
	Hawk	ABC-AED	0.14	0.25	0.16	0.60
	Hawk	Canny	0.12	0.22	0.17	0.32
	House	Hacini	0.00	0.00	0.00	0.00
	House	ABC-AED	0.09	0.16	0.10	0.35
	House	Canny	0.03	0.05	0.03	0.30
2	Hawk	Hacini	0.00	0.00	0.00	0.00
	Hawk	ABC-AED	0.14	0.24	0.16	0.53
	Hawk	Canny	0.02	0.05	0.02	0.38
	House	Hacini	0.00	0.00	0.00	0.00
	House	ABC-AED	0.09	0.16	0.10	0.34
	House	Canny	0.01	0.03	0.01	0.36
3	SEM 1	Hacini	0.01	0.03	0.01	0.94
	SEM 1	ABC-AED	0.04	0.08	0.04	0.93
	SEM 1	Canny	0.00	0.00	0.00	0.00
	SEM 2	Hacini	0.06	0.12	0.06	0.88
	SEM 2	ABC-AED	0.06	0.11	0.06	0.94
	SEM 2	Canny	0.06	0.12	0.07	0.29
	SEM 3	Hacini	0.11	0.20	0.11	0.99
	SEM 3	ABC-AED	0.10	0.18	0.10	0.98
	SEM 3	Canny	0.13	0.24	0.17	0.40
	SEM 4	Hacini	0.14	0.25	0.14	0.92
	SEM 4	ABC-AED	0.11	0.20	0.12	0.91
	SEM 4	Canny	0.25	0.40	0.37	0.43
	SEM 5	Hacini	0.04	0.08	0.04	0.99
	SEM 5	ABC-AED	0.04	0.07	0.04	1.00
	SEM 5	Canny	0.06	0.12	0.09	0.20

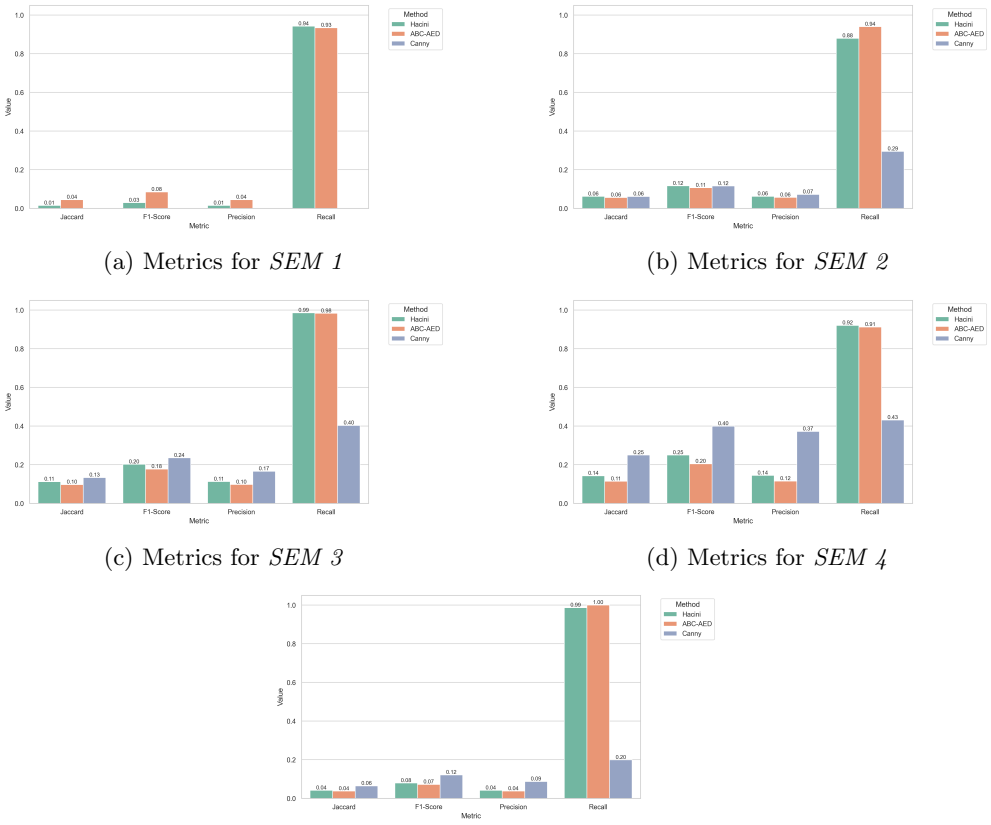
Table 1: Quantitative comparison of edge detection method performance across the three processing stages.

4 Discussion

The comparative analysis carried out across the three stages reveals clear differences in the performance of the edge detection methods depending on the image conditions and the type of perturbation applied.

In Stage 1, focused on the evaluation of natural images without noise, the ABC-AED method demonstrated the best correspondence with the ground truth, presenting higher recall values (0.8267 for Hawk and 0.6873 for House) than those obtained by Canny and the method of [6], indicating its ability to correctly identify the main edges. Although slight contour blurring led to relatively low precision values (0.2135 and 0.1064), the overall edge coverage compensated for this limitation. Canny prioritized the detection of fine details, resulting in higher precision than ABC-AED (0.2948 and 0.0722), but with considerably lower recall, generating more false negatives. The method proposed by [6] showed minimal performance, confirming its limited effectiveness under these conditions.

During Stage 2, in which robustness against noise was evaluated, the vulnerability of Canny became evident: its metrics decreased drastically (e.g., Jaccard values of 0.0409 and 0.0359 for Hawk and House, respectively), reflecting its sensitivity to Gaussian, salt-and-pepper, speckle, and Poisson noise. In contrast, ABC-AED maintained stable performance across all metrics (Jaccard values of approximately 0.21 and 0.099,



(a) Metrics for *SEM 1*

(b) Metrics for *SEM 2*

(c) Metrics for *SEM 3*

(d) Metrics for *SEM 4*

(e) Metrics for *SEM 5*

Fig. 9: Accuracy of the edge maps for the Stage 3 images.

and recall values of approximately 0.76 and 0.56), demonstrating its resilience against different types of noise. The method of [6] continued to show marginal performance, further reinforcing that its applicability is limited to scenarios with clean images and low noise levels.

Finally, in Stage 3, corresponding to SEM images, behavior dependent on the structural complexity of each sample was observed. In SEM images 1 and 2, the ABC-AED method presented the highest recall values (0.93 and 0.94, respectively), outperforming Hacini and evidencing a greater capacity to recover relevant edges; however, this advantage was accompanied by moderate precision values, suggesting the inclusion of spurious detections. In contrast, the Canny operator showed null performance on SEM 1, but progressively improved on images with better-defined edges, achieving the best overall results on SEM 3, SEM 4, and SEM 5. Particularly in SEM 4, Canny obtained the maximum values of Jaccard (0.25), F1-score (0.40), and precision (0.37), indicating a more balanced segmentation between sensitivity and accuracy. For its part, the Hacini method maintained high recall values across all images (0.88–0.99), albeit

accompanied by low precision, reflecting a systematic tendency to over-detect edges. Overall, the results show that ABC-AED favors sensitivity in low-contrast images, while Canny proves more robust when contours exhibit greater spatial definition.

Taken together, the quantitative and qualitative results show that ABC-AED exhibits robust and consistent performance against noise, diffuse edges, and contrast variations, positioning itself as a competitive alternative to classical methods such as Canny and fractional approaches such as that proposed by [6]. Its main limitation corresponds to a slight loss of sharpness in some contours, an aspect that could be mitigated in future work through adaptive post-processing strategies or automatic parameter optimization.

These findings suggest that the choice of method depends on the characteristics of the image being analyzed. In scenes with low contrast or high noise, ABC-AED showed greater stability and edge recovery capacity; in contrast, when contours are better defined, Canny achieved a better balance between precision and recall, attaining in several cases the best overall indicators. Therefore, ABC-AED can be considered a solid alternative under adverse conditions, while Canny retains advantages in images with greater structural definition.

5 Conclusion

The main findings of this study demonstrate the robustness and consistency of the ABC-AED method compared to classical methods and prior fractional approaches, particularly under adverse conditions characterized by noise, low contrast, or diffuse edges.

ABC-AED produced continuous and stable edge maps, reducing the fragmentation observed in some of the compared methods. In tests with noise-free natural images (Stage 1), it achieved the highest Jaccard index and F1-score values in most of the analyzed cases, showing a favorable balance between precision and recall compared to the Canny detector.

The robustness of ABC-AED against noise was particularly noteworthy. The method maintained stable behavior under different types of perturbations, including Gaussian, salt-and-pepper, speckle, and Poisson noise. In contrast, the Canny detector showed greater sensitivity to image degradation, while ABC-AED preserved competitive performance across the evaluated metrics. These results suggest that the smoothing and memory properties associated with the Atangana–Baleanu operator contribute to mitigating noise-induced perturbations.

Furthermore, ABC-AED demonstrated consistent behavior under contrast variations in scanning electron microscopy (SEM) images. In images with faint edges or low contrast, the method maintained effective detection and high recall values, outperforming Canny and the Hacini method in several cases. However, in images with more well-defined contours, the Canny detector achieved the best overall indicators, particularly in terms of Jaccard index, F1-score, and precision. This indicates that ABC-AED offers clear advantages in challenging scenarios, while Canny retains its strengths when the edge structure is better delineated.

The main limitation observed in ABC-AED was a slight smoothing of certain contours, attributable to the intrinsic properties of the fractional operator, which may reduce sharpness in specific regions.

Future research could focus on mitigating this limitation through adaptive post-processing strategies, local enhancement techniques, or automatic parameter tuning procedures. Additionally, the development of hybrid approaches combining the robustness of ABC-AED with spatial refinement methods could further improve edge localization accuracy without compromising its stability against noise.

Supplementary Materials. Not applicable.

Acknowledgements. Not applicable.

Declarations

Some journals require declarations to be submitted in a standardized format. Please check the Instructions for Authors of the journal to which you are submitting to see if you need to complete this section. If yes, your manuscript must contain the following sections under the heading 'Declarations':

- Funding: This research received no external funding.
- Conflict of interest/Competing interests (check journal-specific guidelines for which heading to use): The authors declare no conflict of interest.
- Ethics approval and consent to participate: Not applicable.
- Consent for publication: Not applicable.
- Data availability: The dataset(s) supporting the conclusions of this article are publicly available. The Berkeley Segmentation Dataset is available at: https://doi.org/10.1109/ICCV.2001.937655. The dataset associated with [11] is available at: https://doi.org/10.3390/nano12111818.
- Materials availability Not applicable.
- Code availability: The source code used in this study is publicly available at https://github.com/rnloz26/AdaptativeEdgeDetectorsABC.git.
- Author contribution: All authors contributed equally to this work. All authors read and approved the final manuscript.

If any of the sections are not relevant to your manuscript, please include the heading and write 'Not applicable' for that section.

Editorial Policies for:

Springer journals and proceedings: https://www.springer.com/gp/editorial-policies

Nature Portfolio journals: https://www.nature.com/nature-research/editorial-policies

Scientific Reports: https://www.nature.com/srep/journal-policies/editorial-policies

BMC journals: https://www.biomedcentral.com/getpublished/editorial-policies

Appendix A Algorithms

Algorithm 1 Loading and preprocessing of the SEM image

Require: I ▷ Input image
Ensure: I_G, I_N ▷ Grayscale image, normalized image
1: **if** I is in grayscale **then**
2: $I_G \leftarrow I$
3: $I_N \leftarrow I/255$
4: **else**
5: $I_G \leftarrow \text{GrayScale}(I)$
6: $I_N \leftarrow I_G/255$
7: **end if**

Algorithm 2 Minimum area computation

Require: h, w ▷ Image height and width
Ensure: h_t, w_t ▷ Minimum height and minimum width
1: $h_t \leftarrow h/\gcd(h, w)$ ▷ gcd denotes the greatest common divisor
2: $w_t \leftarrow w/\gcd(h, w)$

Algorithm 3 Adaptive α grid computation

Require: I_N, h_t, w_t
Ensure: α_{grid}

$B \leftarrow \text{Bilateral}(I_N)$ ▷ B is the bilaterally filtered image from I_N
$\text{prod} \leftarrow \mid I_N \times B \mid$
$\alpha_{grid} \leftarrow \mathbf{0_{W \times H}}$ ▷ Zero matrix of the same size as prod
$\alpha_{min} \leftarrow 0.01$
$\alpha_{max} \leftarrow 0.99$
$i \leftarrow 0$
while $i \leq h - h_t$ **do**
    $j \leftarrow 0$
    while $j \leq w - w_t$ **do**
        $\text{area} \leftarrow \text{prod}[i : i + h_t,\ j : j + w_t]$
        $\mu \leftarrow \text{mean(area)}$
        $\alpha \leftarrow \alpha_{min} + (\alpha_{max} - \alpha_{min}) \times \mu$
        $\alpha_{grid}[i : i + h_t,\ j : j + w_t] \leftarrow \alpha$
        $j \leftarrow j + w_t$
    end while
    $i \leftarrow i + h_t$
end while

Algorithm 4 Edge computation

Require: $I_G^{W \times H}$ ▷ Input image
Ensure: G ▷ Gradient magnitude

$h_x \leftarrow 3 \times 3$ matrix
$h_y \leftarrow 3 \times 3$ matrix
$g_x \leftarrow W \times H$ zero matrix
$g_y \leftarrow W \times H$ zero matrix
$x \leftarrow 0$
while $x \leq I.\text{shape}(0) - 2$ **do**
    $y \leftarrow 0$
    while $y \leq I.\text{shape}(1) - 2$ **do**
        $\alpha \leftarrow \alpha_{grid}[x, y]$
        $\text{patch} \leftarrow I[x - 1 : x + 2,\ y - 1 : y + 2]$
        $g_x[x, y] \leftarrow \sum(\text{patch} \times h_x)$
        $g_y[x, y] \leftarrow \sum(\text{patch} \times h_y)$
        $y \leftarrow y + 1$
    end while
    $x \leftarrow x + 1$
end while
$G_x \leftarrow \text{Bilateral}(g_x)$
$G_y \leftarrow \text{Bilateral}(g_y)$
$G \leftarrow \sqrt{G_x^2 + G_y^2}$

References

[1] Ding, Y., Nan, X.: On edge detection algorithms for water-repellent images of insulators taking into account efficient approaches. Symmetry **15**(7), 1418 (2023) https://doi.org/10.3390/sym15071418

[2] Lakshmi, K.T.S., Anil Kumar, R.: An analysis of image segmentation methods. In: Advances in Transdisciplinary Engineering. IOS Press, ??? (2022). https://doi.org/10.3233/ATDE220806 . https://ebooks.iospress.nl/doi/10.3233/ATDE220806

[3] Arora, S., Mathur, T., Agarwal, S., Tiwari, K., Gupta, P.: Applications of fractional calculus in computer vision: A survey. Neurocomputing **489**, 407–428 (2022) https://doi.org/10.1016/j.neucom.2021.10.122

[4] Yaacoub, C., Zeid Daou, R.A.: Fractional order sobel edge detector. In: 2019 Ninth International Conference on Image Processing Theory, Tools and Applications (IPTA) (2019). https://doi.org/10.1109/ipta.2019.8936101

[5] Ghanbari, B., Atangana, A.: Some new edge detecting techniques based on fractional derivatives with non-local and non-singular kernels. Advances in Difference Equations (2020) https://doi.org/10.1186/s13662-020-02890-9

[6] Hacini, M., Hachouf, F., Charef, A.: A bi-directional fractional-order derivative mask for image processing applications. IET Image Processing **14**(11), 2512–2524 (2020) https://doi.org/10.1049/iet-ipr.2019.0467

[7] Wei, T., Wang, X., Li, X., Zhu, S.: Fuzzy subspace clustering noisy image segmentation algorithm with adaptive local variance & non-local information and mean membership linking. Engineering Applications of Artificial Intelligence **110**, 104672 (2022) https://doi.org/10.1016/j.engappai.2022.104672

[8] Rani, G.E., Murugeswari, R., Rajini, N.: Edge detection in scanning electron microscope (sem) images using various algorithms. In: 2020 4th International Conference on Intelligent Computing and Control Systems (ICICCS) (2020). https://doi.org/10.1109/iciccs48265.2020.9121110 . https://doi.org/10.1109/iciccs48265.2020.9121110

[9] Lobato, I., Friedrich, T., Aert, S.V.: Deep convolutional neural networks to restore single-shot electron microscopy images. NPJ Computational Materials **10**(1) (2024) https://doi.org/10.1038/s41524-023-01188-0

[10] Martin, D., Fowlkes, C., Tal, D., Malik, J.: A database of human segmented natural images and its application to evaluating segmentation algorithms and measuring ecological statistics. In: Proceedings of the 8th International Conference on Computer Vision (ICCV), vol. 2, pp. 416–423 (2001). https://doi.org/10.1109/ICCV.2001.937655 . https://doi.org/10.1109/ICCV.2001.937655

[11] López Gutiérrez, J.D., Abundez Barrera, I.M., Torres Gómez, N.: Nanoparticle detection on sem images using a neural network and semi-synthetic training data. Nanomaterials (Basel, Switzerland) **12**(11), 1818 (2022) https://doi.org/10.3390/nano12111818

[12] Atangana, A.: Fractional derivatives, dimensions, and geometric interpretation: An answer to your worries. AIMS Mathematics **10**(2), 2562–2588 (2025) https://doi.org/10.3934/math.2025119

[13] Syam, M.I., Al-Refai, M.: Fractional differential equations with atangana–baleanu fractional derivative: Analysis and applications. Chaos, Solitons & Fractals: X **2**, 100013 (2019) https://doi.org/10.1016/j.csfx.2019.100013

[14] Adams, R.A., Fournier, J.J.F.: Sobolev Spaces: Volume 140, 2nd edn. Pure and Applied Mathematics. Academic Press, San Diego, CA, Estados Unidos de América (2003)

[15] Mainardi, F.: Why the mittag-leffler function can be considered the queen function of the fractional calculus? Entropy **22**(12), 1359 (2020) https://doi.org/10.3390/e22121359 . Basel, Switzerland

[16] Ghanbari, B., Atangana, A.: Some new edge detecting techniques based on fractional derivatives with non-local and non-singular kernels. Advances in Difference Equations **2020**(1) (2020) https://doi.org/10.1186/s13662-020-02890-9

[17] Sonka, M., Hlavac, V., Boyle, R.: Image Processing, Analysis, and Machine Vision, 4th edn. Wadsworth Publishing, ??? (2013)

[18] Lin, C., Yoon, A.P., Wang, C.-W., Chao, T., Chung, K.C., Kuo, C.-F.: Effects of image degradation on deep neural network classification of scaphoid fracture radiographs: Comparison study of different noise types. JMIR Medical Informatics **14**, 65596 (2026) https://doi.org/10.2196/65596

[19] Martin, D., Fowlkes, C., Tal, D., Malik, J.: A database of human segmented natural images and its application to evaluating segmentation algorithms and measuring ecological statistics. In: Proc. 8th Int'l Conf. Computer Vision, vol. 2, pp. 416–423 (2001). https://doi.org/10.1109/ICCV.2001.937655

[20] Bhat, S., Szczuko, P.: Impact of canny edge detection preprocessing on performance of machine learning models for parkinson's disease classification. Scientific Reports **15**(1), 16413 (2025) https://doi.org/10.1038/s41598-025-98356-7

[21] Travieso, G., Benatti, A., Costa, L.d.F.: An analytical approach to the jaccard similarity index. arXiv preprint arXiv:2410.16436 (2024) https://doi.org/10.48550/arXiv.2410.16436